Fabrication, structural and magnetic properties of one-dimensional anti-ferromagnetic FeMn nanostructures

Cite as: AIP Advances **9**, 035225 (2019); https://doi.org/10.1063/1.5079981
Submitted: 05 November 2018 . Accepted: 09 January 2019 . Published Online: 15 March 2019

S. S. Ali, W. J. Li, X. M. Zhang, M. Irfan, J. F. Feng, K. Javed, G. J. Zhai, and X. F. Han

Fabrication, structural and magnetic properties of one-dimensional anti-ferromagnetic FeMn nanostructures

Cite as: AIP Advances 9, 035225 (2019); doi: 10.1063/1.5079981
Presented: 16 January 2019 • Submitted: 5 November 2018 •
Accepted: 9 January 2019 • Published Online: 15 March 2019

S. S. Ali,[1,2] W. J. Li,[1] X. M. Zhang,[1] M. Irfan,[1] J. F. Feng,[1] K. Javed,[3] G. J. Zhai,[4] and X. F. Han[1,a)]

AFFILIATIONS

[1] Institute of Physics, University of Chinese Academy of Sciences, Chinese Academy of Sciences, Beijing 100190, China
[2] Department of Physics, The University of Lahore, Lahore 54000, Pakistan
[3] Department of Physics, Forman Christian College, Lahore 54000, Pakistan
[4] National Space Science Center, Chinese Academy of Sciences, Beijing 100190, China

Note: This paper was presented at the 2019 Joint MMM-Intermag Conference.
[a)] **Corresponding author (email:** xfhan@iphy.ac.cn)

ABSTRACT

FeMn nanowires have been synthesized by employing DC electro-deposition technique provided with constant stirring during the growth. The use of anodic aluminum oxide (AAO) templates made it possible to get well aligned nanowires with average diameter around 100 nm. Magnetic field annealing with field strength of 1 T applied at angle 0° and 90° to nanowires axis at different annealing temperatures has been employed to study the variation in structural and magnetic properties of nanowires. XRD analysis shows poor crystallinity of as-synthesized arrays but cubic structure with (110) preferred orientation has been resulted after the annealing process. Furthermore, vibrating sample magnetometer (VSM) has been employed to study the saturation magnetization (M_s), squareness ratio ($SQ=M_r/M_s$) and coercivity (H_c) of the as-synthesized and annealed samples. The as deposited and annealed NWs arrays show the coherent rotation for magnetization reversal process.

I. INTRODUCTION

The super elasticity and shape memory effect in FeMn and FeMnSi alloys attracted considerable interest for their possible implementation as shape memory alloys in actuators, sensors and in several other potential applications.[1–3] Nano-structured anti-ferromagnetic materials have promising applications in spin valves and the magnetic random access memory (MRAM).[4–8] The spin valve multilayer structures are thought to be potential devices in magnetoresistance read heads in magnetic recording industry. In magnetic recording media the magnetization direction can be stabilized by using the nanostructured anti-ferromagnetic materials.[9–11] Face centered cubic substrate is favorable for the formation of anti-ferromagnetic γ-fcc phase of FeMn which is necessary for exchange bias in spin valve structures.[12–15] Nanowires of anti-ferromagnetic material along with same kind of structure of ferromagnetic material are important in new type of hard magnetic materials. In particular, the properties linked with hysteresis loop can be tuned by changing parameters such as atomic ratio of magnetic alloys, length and diameter of nanowires. FeMn alloy is important because of having no requirement of long and high heat treatments to get transformed in the necessary antiferromagnetic crystallographic structure.[16] Some of the usual methods to fabricate FeMn alloys are sputtering and vacuum plating which have relatively severe experimental conditions and higher cost. Being lower cost and easy to apply, electrochemical deposition method is a good alternative to fabricate such alloys at nanoscale.[12]

Most of the research on antiferromagnetic materials deals with thin film structures and nano-particles but there are very less number of reports on anti-ferromagnetic nanowires.

II. EXPERIMENTAL

For the first time we report FeMn alloy nanowires fabricated by low cost dc electro-deposition method using the nano-channels of porous anodic alumina oxide (AAO) templates with thickness approximately 60 μm. The pore diameter of nano-channels is around 100 nm and the pore density is around 1×10^9 pores cm^{-2}. A 300 nm Cu layer has been sputtered on one side of template to serve as conducting electrode. The electrolytes used for electro-deposition consist of $FeCl_2.4H_2O$, $MnCl_2.4H_2O$ and $(NH_4)_2SO_4$. Citric acid has been added to electrolyte as an inhibitor to prevent oxidation of the ferrous material to ferric material. In the deposition process the Pt strip has been used as counter electrode whereas the sputtered layer and saturated calomel electrode (SCE) served as working and reference electrodes respectively. Synthesis process has been repeated a few times to get the required elemental compositions of deposited product. After the deposition, heat treatment has been given for 2 hours to $Fe_{80}Mn_{20}$ NWs in the presence of magnetic field with fiend strength of 1 T and directions parallel and perpendicular to NWs axis.

III. RESULTS AND DISCUSSION

FIG. 1 shows Field Emission Scanning Electron Microscope (FESEM) image of (a) $Fe_{80}Mn_{20}$ and (b) $Fe_{50}Mn_{50}$ NWs after removing the AAO template. The NWs are well aligned and the average diameter is 100 nm. FIG. 1(c) shows the Energy Dispersive X-ray Spectroscopy (EDX) confirming the deposition of required contents. The extra peak of Cu appeared due to the use of copper tape during the analysis and the Al peak owing to the reason that AAO template has been used in the synthesis process and for this analysis the template has not been removed completely. FIG. 2 indicates the X-Ray Diffraction (XRD) pattern of as deposited $Fe_{80}Mn_{20}$ NWs and those which have been annealed at 400°C in the presence of magnetic field with field direction parallel to NWs axis. XRD analysis reveals that as deposited NWs show very minor crystalline indications or almost amorphous structure. With the heat treatment at the temperature mentioned above an induced crystallinity has been observed and a significant peak of cubic $Fe_{80}Mn_{20}$ alloy with (110) preferred orientation can be seen in XRD pattern. Since the magnetization has an easy axis in the direction of axis of NWs so the magnetic field annealing with field in the direction of NWs axis during the annealing process favors the settlement of more crystallites to be aligned parallel which gives improved crystalline structure and led to better crystallinity giving prominent peak. The standard XRD pattern 04-004-7786 can be taken into account for comparison. In our experiments no significant improvement in crystalline structure has been observed for perpendicular magnetic field annealing case of $Fe_{80}Mn_{20}$ NWs. Vibrating Sample Magnetometer (VSM) has been used to study the magnetic properties of FeMn NWs. FIG. 3(a,b) shows the M-H magnetic

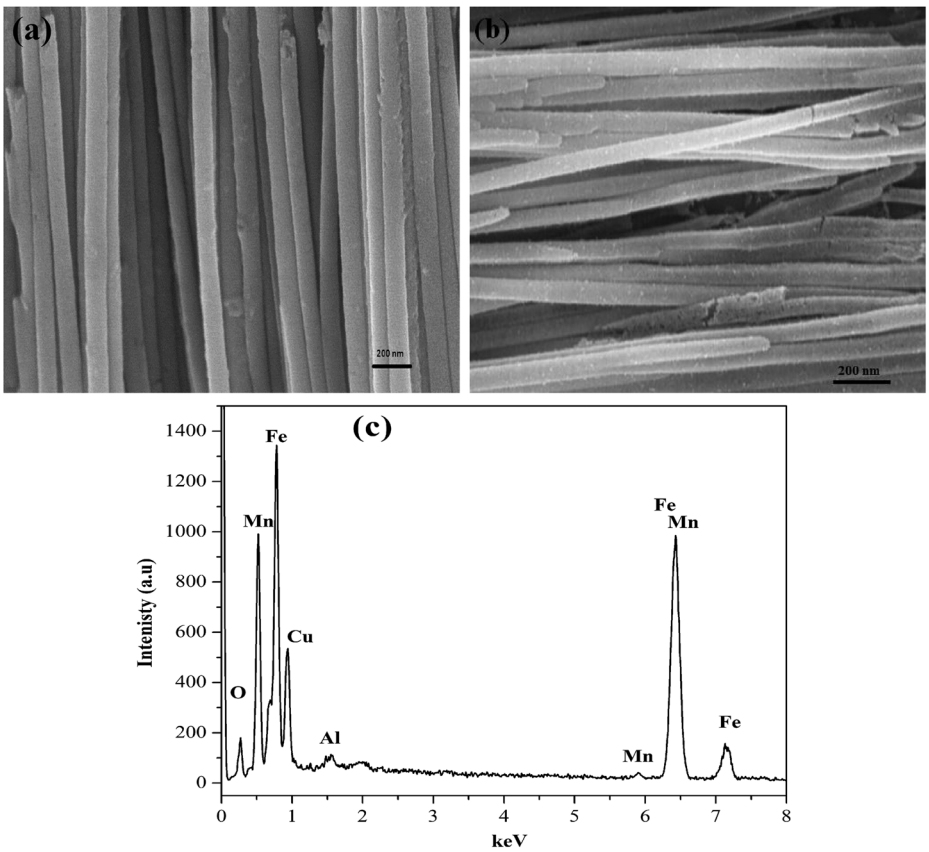

FIG. 1. (a) $Fe_{80}Mn_{20}$ and (b) $Fe_{50}Mn_{50}$ NWs having diameter around 100 nm, (c) EDX analysis of FeMn NWs.

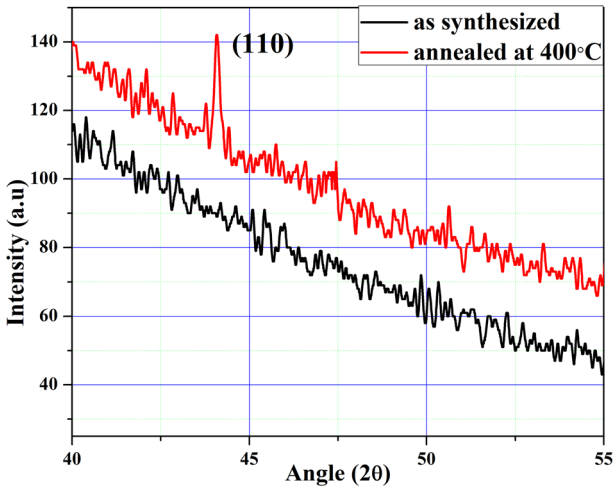

FIG. 2. XRD patterns of as synthesized $Fe_{80}Mn_{20}$ NWs and those annealed at 400°C in the presence of 1 T magnetic field strength applied parallel to NWs during annealing.

hysteresis loops of FeMn NWs composed of different elemental ratios of Fe and Mn. Typical magnetic anisotropic behavior is observed for the $Fe_{80}Mn_{20}$ NWs arrays. The alignment of easy magnetization axis has been observed to be parallel to NWs axis owing to the dominant behavior of shape anisotropy.[17] The overall anisotropic field (H_k) is mainly determined by following three contributions: (1) the shape anisotropy field ($2\pi M_s$), due to which the direction of easy magnetization would be parallel to NWs axis when it has a dominant behavior over the other two contributions of H_k, (2) magneto-static dipole interactions, which causes the easy magnetization axis to get perpendicularly aligned with NWs axis and (3) the magneto-crystalline anisotropy field (H_{ma}) which plays important role for the magnetization reversal mechanism. The relation of effective anisotropic field (H_k) is given as

$$H_k = 2\pi M_s - 6.3\pi M_s r^2 L/D^3 + H_{ma} \quad (1)$$

In this equation the parameters are as follows:
M_s - saturation magnetization,
r - radius of the wire,
L - length of wire,
D - inter-wire distance.[18]

The change in elemental composition significantly changes the magnetic behavior of NWs as shown in the M-H loops measured for different compositions. Antiferromagnetic behavior can be observed for $Fe_{50}Mn_{50}$ NWs as shown for both the cases when external field is applied parallel and perpendicular to the NWs axis. Furthermore with the increase in Fe concentration the ferromagnetic ordering establishes in the structure which gives prominent coercive region in the M-H loop of $Fe_{80}Mn_{20}$ NWs [FIG. 3 (a,b)]. FIG. 4(a) shows the dependence of M_s on annealing temperature when the external magnetic field has been applied in parallel and perpendicular directions. This sample has already been annealed in the presence of magnetic field applied parallel to NWs axis. A symmetric relation for both cases has been observed with an increase to maxima and then decrease to lower values with almost same numerical

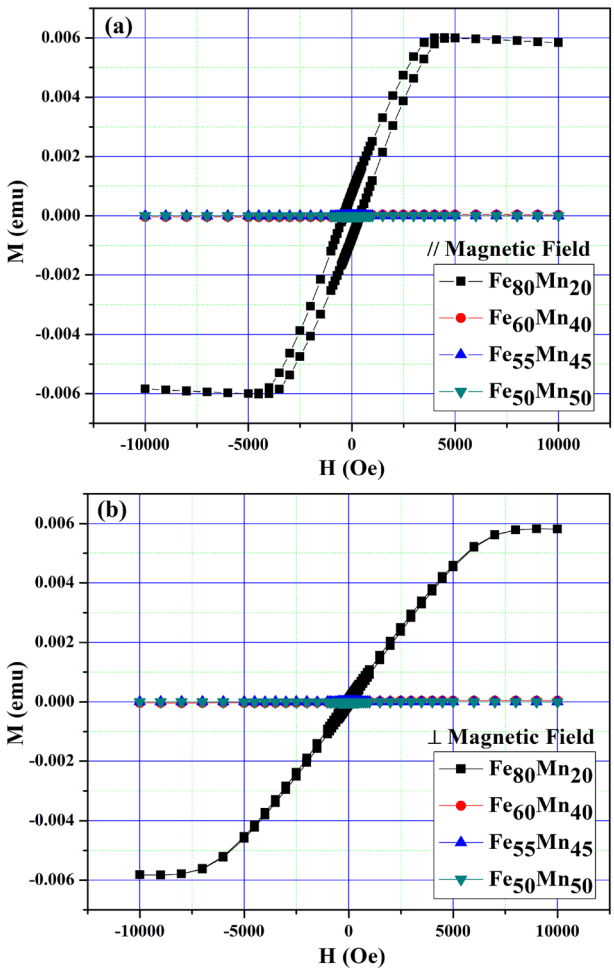

FIG. 3. M-H loops of FeMn nanowires with different elemental compositions when (a) field applied parallel to NWs axis and (b) field applied perpendicular to NWs axis.

values for both easy and hard magnetization axes. The increase in M_s with MF annealing temperature up to 200°C is attributed to the better alignment of magnetic moments. Since the easy magnetization axis is along the nanowires axis due to dominant behavior of shape anisotropy therefore the heat treatment with magnetic field in the direction of easy magnetization axis makes it favorable to get more magnetic moments aligned in the mentioned direction and of course this results in the form of improved magnetic behavior. The magnetic characteristics of nanowires are affected on providing magnetic field assisted heat treatment due to stress relief between the grains and directional atomic pair ordering. This treatment may further causes decrease in dipole magneto-static interactions and self-demagnetizing fields of the wires due to the redistribution of pair directions perpendicular to magnetization in each domain leading to a considerable increase in M_s values. Furthermore, with the increase in annealing temperature there occurred a decrease in M_s values. Although there can be several mechanisms responsible for this decrease in M_s however in each case there must

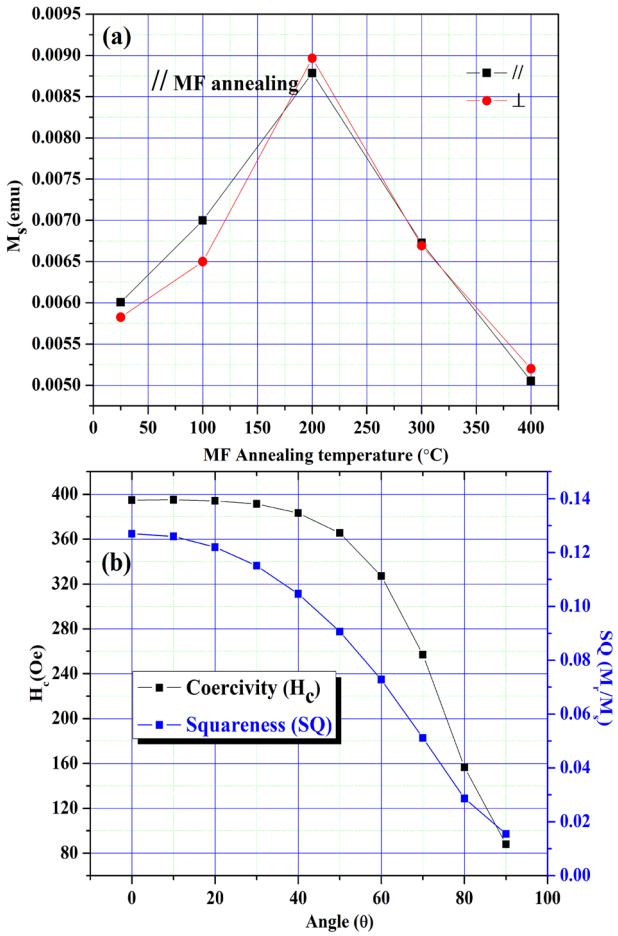

FIG. 4. (a) M_s dependence on magnetic field annealing temperature, (b) variation in H_c and SQ with increasing angle of applied magnetic field.

be loss of free Fe atoms. The very small dimensional parameters of nanostructures cause a decrease in their melting point as compared when they are in bulk quantity.[19–21] On the basis of these facts, one of the possible reasons of decrease in M_s at higher temperature can be the incorporation of electrodeposited $Fe_{80}Mn_{20}$ NWs with the inside walls of nano-pores of AAO template. This incorporation can result in formation of nonmagnetic compound which leads to interface defects and causes a decrease in M_s. Another possible reason of decrease in M_s at higher temperatures is the formation of anti-ferromagnetic regions within the NWs in which magnetic Fe atoms are captured in regions with Mn atoms which leads to rapid fall in M_s. FIG. 4 (b) shows the variation in H_c and SQ with the change in direction of external magnetic field. The commonly studied magnetization reversal processes are the coherent rotation and curling rotation of magnetization. The diameter at which the coherent rotation switches to curling is $d_c = 2.08(A^{1/2}/M_s)$, Where, A is exchange stiffness and M_s is saturation magnetization.[22] The curling mode of magnetization reversal dominates when the diameter exceeds with the critical diameter. The relation which links the H_c with the angle for the magnetization reversal mechanism is given as.[23]

$$H_c = \frac{a(1+a)}{\sqrt{a^2 + (1+2a)\cos^2\theta}} H_k \qquad (2)$$

where $a = -1.08(d_c/d)^2$. A directly proportional link in H_c and θ shows the curling rotation of magnetic domains. In our case the magnetization reversal mechanism is the other one, i.e the coherent mode of magnetization reversal where the maximum and the minimum H_c values are found when the field is applied at angle 0° and 90° with the axis of NWs respectively. The coherent rotation of magnetic domains for 100 nm $Fe_{80}Mn_{20}$ NWs [FIG. 4(b)] can be explained by taking an account of interwire coupling among the NWs arrays. The magneto-static interactions among the NWs play an important role for magnetization reversal mechanism. Since the interpore distance of AAO template in our case is very small i.e, about 15 nm which gives significant interwire coupling among the NWs and leads to the parallel alignment of moments of adjacent wires. In this case the total energy is smaller and the interaction favors the coherent mode of magnetization reversal.

IV. CONCLUSIONS

In conclusion nano-template assisted electro-deposition technique has been employed to fabricate FeMn NWs with diameter of about 100 nm. Different elemental compositions have been produced and particularly antiferromagnetic ordering $Fe_{50}Mn_{50}$ has been achieved. The $Fe_{80}Mn_{20}$ NWs arrays subjected to heat treatment at different annealing temperatures in the presence of 1 T magnetic field strength. The as-synthesized NWs show poor crystallinity which gets improved at higher annealing temperatures and cubic crystalline phase with (110) preferred orientation has been observed. Variation in magnetic properties including H_c, SQ and M_s with increasing annealing temperature has been discussed with the increase of annealing temperature. Furthermore, coherent mode of magnetization reversal mechanism has been observed due to significant inter-wire couplings at the cost of smaller inter-wire distances among NWs arrays.

ACKNOWLEDGMENTS

This work was supported by the National Key Research and Development Program of China [MOST, Grants No. 2017YFA0206200], the National Natural Science Foundation of China [NSFC, Grants No. 11434014 and No. 51831012], NSFC-PSF joint project [NSFC No. 51761145110], and partially supported by the Strategic Priority Research Program (B) [Grant No. XDB07030200], the International Partnership Program (Grant No. 112111KYSB20170090), and the Key Research Program of Frontier Sciences (Grant No. QYZDJ-SSWSLH016) of the Chinese Academy of Sciences (CAS).

REFERENCES

[1] T. Jurgeleit, L. K. Jessen, E. Quandt, and C. Zamponi, Materials **11**, 482 (2018).
[2] M. Formentini and S. Lenci, Automation in Construction **85**, 220 (2018).
[3] M. Wiesener, K. Peters, A. Taube, A. Keller, K. P. Hoyer, T. Niendorf, and G. Grundmeier, Materials and Corrosion **9999**, 1 (2017).
[4] V. V. Ustinov, M. A. Milyaev, and L. I. Naumova, Physics of Metals and Metallography **118**, 1300 (2017).

[5]Z. Feng, J. W. A. Robinson, and M. G. Blamire, Appl. Phys. Lett. **111**, 042602 (2017).
[6]S. Shirotori, S. Hashimoto, M. Takagishi, Y. Kamiguchi, and H. Iwasaki, Appl. Phys. Express **8**, 023103 (2015).
[7]U. D. C. Hernandez, M. A. Sousa, F. J. Litterst, V. P. Nascimento, and E. B. Saitovitch, J. Magn. Magn. Mater. **390**, 114 (2015).
[8]X. F. Han, Z. C. Wen, and H. X. Wei, J. Appl. Phys. **103**, 07E933 (2008).
[9]N. Banerjee, C. B. Smiet, R. G. J. Smits, A. Ozaeta, F. S. Bergeret, M. G. Blamire, and J. W. A. Robinson, Nat. Commun. **5**, 3048 (2014).
[10]A. Paul, M. Buchmeier, D. E. Burgler, and P. Grunberg, J. Magn. Magn. Mater. **286**, 258 (2005).
[11]V. Skumryev, S. Stoyanov, Y. Zhang, G. Hadjipanayis, D. Givord, and J. Nogues, Nature **423**, 850 (2003).
[12]P. Liu, C. Yao, W. Zhang, Q. Yang, G. Li, Y. Tong, and G. A. Hope, Thin Solid Films **516**, 3935 (2008).
[13]S. Blomeiera, D. Mc Groutherb, R. O'Neillb, S. Mc Vitieb, J. N. Chapmanb, M. C. Webera, B. Hillebrandsa, and J. Fassbenderc, J. Magn. Magn. Mater. **290**, 731 (2005).
[14]S. P. Hao, Y. X. Suib, R. Shana, L. Sunc, and S. M. Zhoua, Thin Solid Films **485**, 212 (2005).
[15]K. Wolfgang, L. I. Chelaru, O. Francesco, W. Jing, K. Masato, and K. Jurgen, Phys. Rev. Lett. **92**, 017201 (2004).
[16]F. Garcia, G. Casali, S. Auffret, B. Rodmacq, and B. Dieny, J. Appl. Phys. **91**, 6905 (2002).
[17]X. F. Han, S. Shamaila, R. Sharif, J. Y. Chen, H. R. Liu, and D. P. Liu, Adv. Mater. **21**, 4619 (2009).
[18]S. Shamaila, R. Sharif, S. Riaz, M. Ma, M. Khaleeq-ur-Rahman, and X. F. Han, J. Magn. Magn. Mater. **320**, 1803 (2008).
[19]D. Mauri, H. C. Siegmann, P. S. Bagus, and E. Kay, J. Appl. Phys. **62**, 7 (1987).
[20]V. Baltz, J. Sort, S. Landis, B. Rodmacqand, and B. Dieny, PRL **94**, 117201 (2005).
[21]J. L. Wang, Phys. Rev. B. **66**, 085408 (2002).
[22]H. Zeng, R. Skomski, L. Menon, Y. Liu, S. Bandyopadhyay, and D. J. Sellmyer, Phys. Rev. B **65**, 134426 (2002).
[23]W. F. Brown, Phys. Rev. **105**, 1479 (1957).